Carbazole Green and Blue-BODIPY Dyads and Triads as Donors for Bulk Heterojunction Organic Solar Cells

Jian Yang, Charles H. Devillers, Paul Fleurat-Lessard, Hao Jiang, Shifa Wang, Claude P Gros, Gaurav Gupta, Ganesh D Sharma, Haijun Xu

Carbazole Green and Blue-BODIPY Dyads and Triads as Donors for Bulk Heterojunction Organic Solar Cells

Jian Yang,[a,b] Charles H. Devillers,[b] Paul Fleurat-Lessard,[b] Hao Jiang,[a] Shifa Wang,[a] Claude P. Gros,[b*] Gaurav Gupta[c], Ganesh D. Sharma,[c*] and Haijun Xu,[a*]

[a]Jiangsu Co-Innovation Center of Efficient Processing and Utilization of Forest Resources, College of Chemical Engineering, Nanjing Forestry University, Nanjing 210037, China. e-mail: xuhaijun@njfu.edu.cn.
[b]Institut de Chimie Moléculaire de l'Université de Bourgogne, UMR CNRS 6302, Université Bourgogne Franche-Comté, 9, Avenue Alain Savary, BP 47870, 21078 Dijon cedex, France. e-mail: Claude.Gros@u-bourgogne.fr
[c]Department of Physics, LNM Institute of Information Technology, Rupa ki Nagal, Jamdoli, Jaipur 302031, Rajasthan, India. e-mail: gdsharma273@gmail.com

Abstract

Two BODIPY derivatives with one (**B2**) and two (**B3**) carbazole moieties were designed, synthesized and applied as electron-donor materials in organic photovoltaic cells (OPV). The optical and electrochemical properties were systematically investigated. These BODIPY dyes exhibit excellent solubility in organic solvents and present high molar extinction coefficients (1.37–1.48 x 10^5 M^{-1} cm^{-1}) in solutions with absorption maxima at 586 nm for mono-styryl group and at 672 nm for di-styryl groups. The introduction of the styryl moieties result in a large bathochromic shift and a significant decrease in the HOMO-LUMO energy-gaps. The BODIPY dyes show relatively low HOMO energies ranging from -4.99 to -5.16 eV as determined from cyclic voltammetry measurements. Cyclic voltammetry measurements and theoretical calculations demonstrate that the frontier molecular orbital levels of these compounds match with $PC_{71}BM$ as the acceptors, supporting their application as donor materials in solution-processed small molecule bulk heterojunction (BHJ) organic solar cells. After the optimization of the active layer, **B2**:$PC_{71}BM$ and **B3**:$PC_{71}BM$ based organic solar cells showed the overall power conversion efficiency of 6.41% and 7.47%, respectively. The higher PCE of **B3** based OSC is ascribed to the more balanced charge transport and exciton dissociation, better crystalline and molecular packing.

1. Introduction

Solar cells have attracted considerable attention as renewable and environmentally friendly energy sources due to environmental issues and the increasing energy crisis resulting from the exhaustion of petroleum resources.[1, 2] During the development of solar energy conversion technology, silicon solar cells are commercial predominant photovoltaic technologies.[3] However, Organic Solar Cells (OSCs), based on a bulk heterojunction (BHJ) structure typically consisting of a blend of a photoactive polymer or a small molecule as an electron donor and fullerene derivatives as an electron acceptor, are being a promising technology to convert solar energy into electricity. They have shown to be relevant candidates for next generation renewable energy convertors owing to some unique merits such as transparency, low cost, flexibility, copious availability, large area, uncomplicated fabrication, and light weight.[4-9] Over the past decades, both Small-Molecule based OSCs (SM-OSCs) and polymer-based organic solar cells have shown a good performance in bulk hetero-junction organic solar cell devices.[10-12] Recently, the polymer-based OSCs as donor have made significant progress with an outstanding efficiency of more than 13%, which represents a great progress for future successful commercialization of OSCs.[13-16] Although the polymer solar cells are very promising in the development of solar energy conversion devices, the drawbacks of polymer OSCs such as chain-length polydispersity, low batch-to-batch reproducibility, structural defects, and possible difficulties in purification still remarkably limit their application in industrial scale.[3, 9, 17] On the other hand, compared to organic polymers, small organic molecules are preferred to be utilized as photoactive electron donors due to their potential advantages such as facile purification and characterization, definite molecular structure and molecular weight, high purity and good batch-to-batch reproducibility.[9, 17-19] In addition, absorption spectra and orbital energy levels of small organic molecules can be fine-tuned with suitable structural modifications so as to match the device characteristics to a

specific given acceptor, which is very difficult in polymer solar cells.[9] Recently, great efforts have been made to raise Power Conversion Efficiencies (PCEs) of small organic molecule OSCs.[20-22] To date, OSCs based on a small molecule as a donor have reached efficiencies in the range of 10–12%,[11, 21] which has made it closer to commercial viability.[23-25] However, new ideal small molecule materials are still in great need to further improve the PCEs and device durability, which are crucial for the commercialization of this technology.[26] Therefore, it is worthwhile to investigate new small organic molecules for application in bulk heterojunction solar cells.

Based on the distinguishing properties of BODIPY and carbazole, in order to develop a promising BODIPY based small molecule for high efficiency OSC, we have designed and synthesized two carbazole–BODIPY based dyes (**B2** and **B3**, Scheme 1) by Knoevenagel condensation reaction. The optical properties, electrochemical behavior and photovoltaic performances of these styryl substituted BODIPY dyes were investigated and the influence of donor's electron donating ability and substituted positions on their electronic and photovoltaic properties were also comparatively investigated.

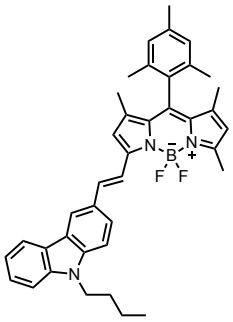

B-2

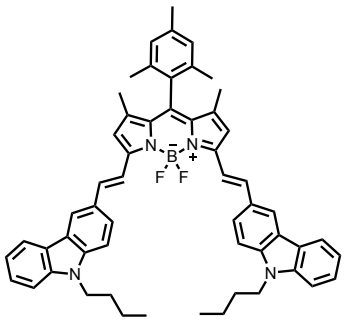

B-3

Scheme 1. Chemical structures of **B2** and **B3**

Employing the $PC_{71}BM$ as acceptor and these two BODIPY based small molecules as donor, the OSCs based on **B2**:$PC_{71}BM$ and **B3**:$PC_{71}BM$ BHJ active layers showed overall PCE of 6.41% (J_{sc} = 13.48 mA/cm^2, V_{oc} = 0.78 V and FF= 0.61) and 7.47% (16.18 mA/cm^2, V_{oc} = 0.71 and FF = 0.65), respectively.

2. Experimental Section

2.1. General

All chemicals and solvents were of analytical reagent grade and used directly as received unless otherwise noted. Dry CH_2Cl_2 was distilled from CaH_2 under nitrogen. ^1H and ^{13}C NMR spectra were collected on a Bruker DRX-600 AVANCE III spectrometer. Chemical shifts for ^1H NMR spectra were recorded in ppm relative to $CDCl_3$ (δ = 7.26 ppm) as the internal standard. Mass spectra data were obtained using a Thermo Fisher LTQ Orbitrap XL (HR-ESI) spectrometer.

2.2. Synthesis

B1 was synthesized according to the reported literature[27] and **C1** was synthesized according to the reported literature.[28]

2.3. Electrochemistry

CH_2Cl_2 was dried over alumina cartridges using a solvent purification system PureSolv PS-MD-5 model from Innovative Technology and kept under argon. Tetraethylammonium tetrafluoroborate ($TEABF_4$) was purchased from Alfa Aesar and recrystallized in MeOH. Electrochemical measurements were performed in CH_2Cl_2 under an Ar atmosphere in a three-electrode glass cell. Working electrode (WE) was a platinum (Pt) disk (Ø = 1 mm, surface area of about 0.785 mm²). A Pt wire was used as counter electrode (CE). Saturated aqueous calomel (SCE) was used as reference electrodes (RE). The RE was separated from the WE compartment by a double frit comprising an intermediate background solution (0.1 M $TEABF_4$ + CH_2Cl_2). All the potentials in this manuscript are indicated *vs*. SCE. In these conditions, when operating in CH_2Cl_2 (0.1 M $TEABF_4$), the formal potential for the Fc^+/Fc couple was found to be +0.52 V *vs*. SCE. All the electrochemical studies were performed using Autolab PGSTAT 302N potentiostat. Cyclic voltammetry experiments were performed at the scan rate of 100 mV/s.

2.4. Synthesis

Synthesis of compounds **B2** and **B3**

In a 50 ml three-neck round bottom flask with a Dean-Stark apparatus, **B1** (3 mmol, 1098 mg), **C1** (3 mmol, 754 mg), *p*-toluenesulfonic acid (0.87 mmol, 150 mg), toluene (25 ml) and piperidine (2 ml) were added. After heating to reflux, the progress of the reaction was monitored by TLC, the reaction was stopped until **B1** disappeared completely. The mixture was cooled to room temperature, which was washed twice with brine, and extracted three times with dichloromethane. The combined organic phase was dried over anhydrous Na_2SO_4

and the solvent was evaporated on a rotary evaporator under reduced pressure. The resulting crude residue was purified by silica gel column chromatography, eluted with CH_2Cl_2/petroleum ether = 6:4, giving **B2** (214.7 mg, 12%) and **B3** (318.2 mg, 13%). **B2**: ^{1}H-NMR (600 MHz, $CDCl_3$, ppm)：δ 8.29 (s, 1H), 8.17 (d, *J* = 7.2 Hz, 1H), 7.79-7.73 (m, 2H), 7.48 (t, *J* = 8.4 Hz, 2H), 7.42-7.38 (m, 2H), 7.29-7.26 (m, 1H), 6.97 (s, 2H), 6.66 (s, 1H), 5.99 (s, 1H), 4.32 (t, *J* = 6.0 Hz, 2H), 2.64 (s, 3H), 2.36 (s, 3H), 2.14 (s, 6H), 1.90-1.86 (m, 2H), 1.47 (s, 3H), 1.44-1.39 (m, 5H), 0.97 (t, *J* = 7.2 Hz, 3H). ^{13}C NMR (150 MHz, $CDCl_3$, ppm): δ 153.81, 141.98, 141.13, 140.97, 140.93, 139.49, 138.52, 137.90, 135.29, 132.18, 131.37, 130.69, 128.93, 127.80, 125.98, 125.55, 123.30, 122.91, 120.72, 120.48, 120.28, 119.36, 117.26, 116.35, 109.06, 108.99, 43.02, 31.17, 21.24, 20.57, 19.64, 14.77, 13.90, 13.73, 13.38. HRMS (ESI): (M^+, $C_{39}H_{40}BF_2N_3$) calculated: 599.3283; found: 599.3307 (M^+). **B3**: ^{1}H-NMR (600 MHz, $CDCl_3$, ppm): δ 8.34(s,2H), 8.22 (d, *J* = 7.2 Hz, 2H), 7.86-7.83 (m, 4H), 7.50 (t, *J* = 7.2 Hz, 4H), 7.44-7.42 (m, 4H), 7.29 (t, *J* = 7.2 Hz, 2H), 6.98 (s, 2H), 6.70 (s, 2H), 4.34 (t, *J* = 7.2 Hz, 4H), 2.37 (s, 3H), 2.17 (s, 6H), 1.92-1.87 (m, 4H), 1.49 (s, 6H), 1.47-1.41 (m, 4H), 0.98 (t, *J* = 7.2 Hz, 6H). ^{13}C NMR (150 MHz, $CDCl_3$, ppm): δ 152.75, 141.08, 140.95, 140.78, 138.49, 137.26, 137.20, 135.65, 132.38, 131.56, 128.88, 128.10, 125.96, 125.63, 123.34, 123.00, 120.77, 120.24, 119.35, 117.17, 116.73, 109.10, 109.00, 43.04, 31.19, 21.17, 20.60, 19.76, 13.92, 13.71. MS (ESI): (M^+, $C_{56}H_{55}BF_2N_4$) calculated: 832.4488; found: 832.4525 (M^+).

2.5. Device fabrication and characterization

The solution processed organic solar cells were fabricated on the ITO coated glass substrate. The ITO coated glass substrates were cleaned in detergent, and subsequently ultra-sonicated in deionized water, acetone and isopropyl alcohol and dried *in vacuum* oven to remove all the traces of residues. For each molecule, the photovoltaic performance optimization process was started with identifying the donor to acceptor ratio (weight percentage, varying from 1:05 to

1:2) and after that solvent vapor annealing was applied to maximize the performance of the OSCs. The $PC_{71}BM$ was used as acceptor and the total concentration of D:A blend mixture was 16 mg/mL in chloroform. The devices were fabricated by depositing PEDOT:PSS as hole transport layer having thickness of 35-40 nm. The active layer was deposited by spin coating (2500 rpm, 60 s) on the top of PEDOT:PSS layer under ambient conditions. For the solvent vapor annealing (SVA), the optimized (as cast 1:1.5 D/A wt ratio) was exposed to the THF vapors for 40s. A thin layer of PFN was spin coated on the top of the active layer from the methanol solution. The aluminum (Al) electrode was deposited onto the top of PFN layer *via* thermal evaporation at the pressure less than 10^{-5} Torr. The current-voltage characteristics of the OSCs were measured under illumination intensity of 100 mW/cm^2 (AM1.5 G) using a solar simulator and a Keithley 2400 source meter unit. The incident photon to current conversion efficiency (IPCE) measurements were performed using Bentham IPCE system.

2.6. Computational details

Quantum mechanics calculations were performed with the Gaussian16 software package.[29] Energy and forces were computed by density functional theory with the M06-2X exchange-correlation functional,[30] with the Pople 6-31G(d,p) basis sets. Geometry optimizations were conducted with the default criteria. Frequency calculations were performed to confirm that all structures were minimized.

2.7 Spectroscopic measurements.

UV-vis spectra were carried out on a Shimadzu UV-3100 spectrophotometer. All the Spectra and PLQY were measured in Fluoro Log-Ultra-Fast (HORIBA Instrument Inc, Edison) equipped with a 450 W CW Xenon lamp and an Open-Electrode TECooled CCD Detector (Syncerity). Absorption and emission measurements were carried out in 1×1 cm quartz cuvettes with spectroscopic grade solvent, and was kept constant at (298 ± 2) K. An integrating sphere mounted in sample compartment directly for PLQY measure. Nanosecond

lifetime and TRES studies were conducted using a TCSPC MCA model equipped with a picosecond photo detector (<200 ps) (PPD850) and picosecond laser (duration is 180 ps, Deltadiode, 100 MHz laser). TRES data were measured by incrementing the monochromator on the emission channel of the time-resolved fluorometer in fixed wavelength intervals at each wavelength. Slices of data were taken in the intensity-wavelength plane to obtain spectra at different times during the decay. Microsecond lifetime decays were collected by a MCS mode on TCSPC HUB (Delta HUB) with a LED source (Spectra LED) as a sample excitation source.

3. Results and discussion

Among the various types of small molecule photovoltaic materials, 4,4-difluoro-4-bora-3a,4a-diaza-s-indacene (BODIPY) dyes have attracted tremendous interest and have been considered to be excellent photoelectric materials owing to their outstanding photophysical properties, such as high molar extinction coefficients, high fluorescence quantum yields, excellent chemical stability, various redox activity, relatively long excited state lifetimes, high thermal and photo-stabilities,[31-33] which have led to their application in many fields including bioimaging,[34, 35] nonlinear optics,[36, 37] photodynamic therapy,[38] organic light-emitting diode,[39, 40] dye-sensitized solar cells (DSSC)[2, 41, 42] and OSCs.[1] In addition, BODIPY derivatives are easily synthesized, and their photophysical and electrochemical characteristics can be easily fine-tuned though an appropriate synthetic modification on the BODIPY core.[43-46] For example, the absorption wavelength of the BODIPY dyes can be finely adjusted by introducing different functional groups at the α, β or *meso*-positions.[27, 47] Moreover, BODIPY dyes can also exhibit variable redox chemistry by selectively accessing a group having a corresponding function, and they have been used as both electron donors and acceptors.[48-50] Considering these outstanding advantages, BODIPY dyes can served as potent candidates for bulk heterojunction solar cells.[1, 7] In 2009, Roncali *et al.* first reported the use of BODIPY

dyes as donor materials and [6,6]-phenyl C_{61}-butyric acid methyl ester ($PC_{61}BM$) as electron acceptor in BHJ-OSCs with a PCE of 1.34%.[51] Since then, continuous progress has been done on BODIPY dyes using them as donors in bulk heterojunction (BHJ) solar cells.[7, 17, 52-62] In 2016, Liao *et al.* synthesized and characterized a series of novel BODIPY derivatives with various electron donors at 2,6-positions for BHJ-OSCs, and the best device exhibits 2.15% PCE.[63] In 2017, Singh *et al.* reported a novel boron dipyrromethene based dye decorated with dithiafulvalene wings and its bulk heterojunction solar cells with $PC_{71}BM$ have achieved a PCE of 7.2%.[61] In 2018, Li *et al.* reported three furan-fused BODIPY with increasing perfluorinated alkyl chains on the *meso*-C of BODIPY core, and an encouraging PCE of 6.4%, with a high FF of 64%, was achieved with C_{60} as the electron acceptor.[62] Recently, Gros *et al.* have designed and synthesized two novel small molecules consisting of a BODIPY central core surrounded by two DiketoPyrroloPyrrole (DPP) and two porphyrin units.[3] The resulting molecule **BD-tPor** presented an impressive PCE of 8.98% when blend with $PC_{71}BM$ as an acceptor for solution processed bulk heterojunction organic solar cells.[3] More recently, Sobral *et al.* have designed three novel BODIPY-based molecules with different styryl aromatic donor group and constructed OSCs with $PC_{60}BM$, which lead to a PCE of 2.8%.[64] Very recently, Singh *et al.* reported two efficient donor materials composed by the dithienosilole/dithienogermole core linked thienyl BODIPY, and the best PCE of 4.58% was achieved.[9] These encouraging results suggest that the BODIPY derivatives have emerged as promising photovoltaic materials. On the other hand, carbazole derivatives have attracted considerable attention in the field of optoelectronics owing to their low redox potential, high hole transport properties, coplanar configuration, and strong electron donating ability.[58] The introduction of carbazole donating unit on D-A organic semiconductors, lowering the HOMO energy level, results in high open circuit voltage in OSCs.[65, 66] In addition, the introduction of carbazole groups into the BODIPY unit can not only improve the photoelectric properties but

also result in the remarkable red shifted absorption spectra and better hole transport.[67] Zhang *et al.* have designed star shaped carbazole-BODIPY derivatives and employed them as donors in BHJ organic solar cells and reported a moderate PCE of 2.70% with a high V_{oc} of 0.85 V.[68] In 2015, Sharma *et al.* used three carbazole substituted BODIPYs small molecules as donors along with $PC_{71}BM$ as an electron acceptor to construct solution processed BHJ organic solar cells, which achieved a PCE at 5.08%.[58]

3.1. Synthesis

BODIPY **B1** was synthesized according to the literature.[27] Compounds **B2** and **B3** were prepared by a Knoevenagel condensation reaction between **B1** and *p*-methoxybenzaldehyde in the presence of 4-methylbenzenesulfonic acid (PTSA) and piperidine in toluene (Scheme 2). The structures of the synthesized compounds were further confirmed by ^{1}H NMR and ^{13}C NMR spectroscopy and HRMS (ESI).

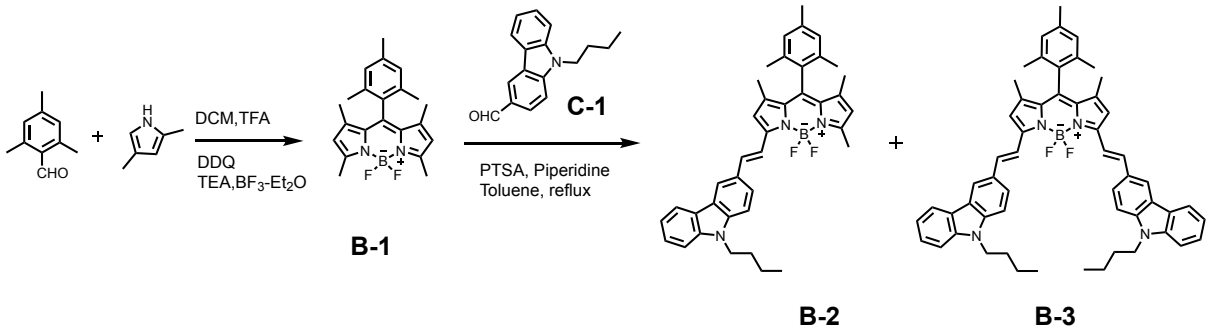

Scheme 2. Synthetic route of **B2** and **B3**

3.2. Electrochemistry

Table 1. Redox potentials *vs.* Fc^{+}/Fc ($E_{1/2} = (E_{pa} + E_{pc})/2$) of **B2** and **B3** ($CH_2Cl_2$ 0.1 M $TEABF_4$, C=10^{-3} M, v = 100 mV/s, working electrode: platinum disk, Ø = 1 mm, counter electrode: Pt wire, reference electrode: SCE); ΔE_p (in mV) are given in parentheses.

Potentials V *vs.* Fc/Fc^{+}	**Red1**	**Ox1**	**Ox2**	**Ox3**	**Δ*E*(Ox1−Red1)** ≈HOMO-LUMO gap
B2	−1.625 (90)	0.365 (80)	0.645 (80)		1.99
B3	−1.53 (85)	0.19 (80)	0.43 (80)	1.12[a]	1.72

[a] Irreversible peak, measurable peak potential.

The cyclic voltammetry curves and differential pulse voltammetry data of **B2** and **B3** are presented in Figure 1 and Figure 2, respectively. Electrochemical data from Table 1 were used to assess frontier orbital energy levels (Table 2). The HOMO and LUMO energy levels were estimated by using the following equations: HOMO = -(4.8 + $E_{1/2}$(Ox1)) and LUMO = -(4.8 + $E_{1/2}$(Red1)) according to Cardona *et al.*[69] and Wang *et al.*[70] **B1** has already been studied in similar conditions as for **B2** and **B3**[71] and its measured HOMO-LUMO gap was 2.33 eV. Among **B2** and **B3** derivatives**, B2** exhibits the highest HOMO-LUMO band gap (1.99 eV, Table 1) due to a lower extension of the π-system (see Figure 5). However, this value is lower than the one found for **B1** proving the significant π-conjugation between the additional carbazole moiety and the BODIPY moiety. When the BODIPY is connected to two carbazole units (**B3**), the HOMO-LUMO gap dropped to 1.72 eV.

Table 2. Frontier orbital energies of **B2** and **B3** in solution as determined by electrochemical data from Table 1.

Compounds	$E_{1/2}$(Ox1) V *vs.* Fc^+/Fc	$E_{1/2}$(Red1) V *vs.* Fc^+/Fc	HOMO (eV)	LUMO (eV)	HOMO-LUMO gap (eV)
B2	0.365	−1.625	−5.165	−3.175	1.99
B3	0.19	−1.53	−4.99	−3.27	1.72

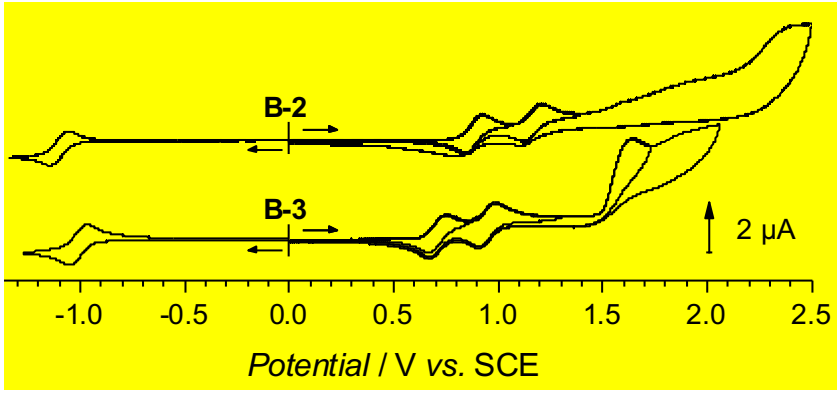

Figure 1. Cyclic voltammetry of **B2** and **B3** in CH_2Cl_2 0.1 M $TEABF_4$ ($c = 10^{-3}$ M, v = 100 $mV.s^{-1}$, WE: Pt, $\varnothing$ = 1 mm).

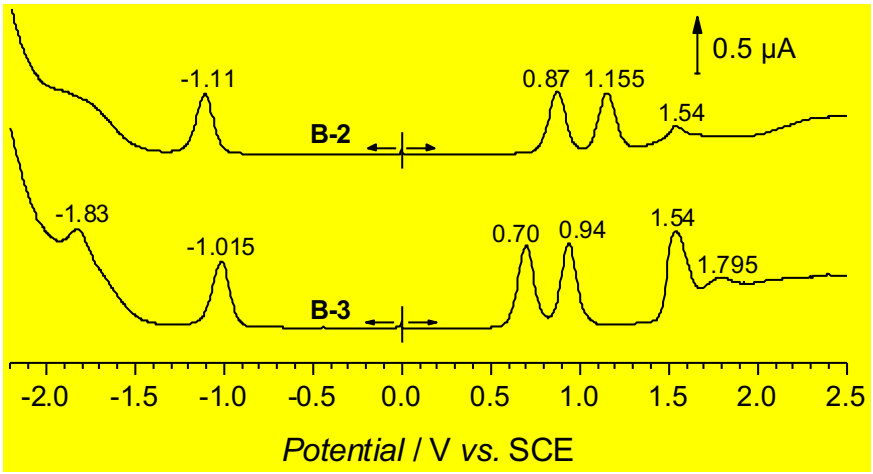

Figure 2. Differential pulse voltammetry of **B2** and **B3** in CH_2Cl_2 0.1 M $TEABF_4$ ($c = 10^{-3}$ M, $v = 10$ mV.s^{-1}, WE: Pt, $\varnothing = 1$ mm).

The better LUMO and HOMO offsets between donors (**B2** and **B3**) and $PC_{71}BM$ (higher than the threshold value of ~0.3 eV) is beneficial for the efficient photo-induced charge transfer at D/A interfaces and transport in the BHJ active layers.[72]

3.3. Optical properties

The photophysical properties of the BODIPY compounds **B2** and **B3** were measured in CH_2Cl_2. The normalized absorption and fluorescence spectra of compounds **B2** and **B3** are shown in Figures 3 and 4, respectively. Their photophysical data are summarized in Table 3. The two BODIPY dyes exhibit classic absorption and emission spectra for BODIPY fluorophores.[73, 74] Compound **B2** shows the maxima absorption with the sharp S_0–S_1 (π–π^*) transition at 586 nm. By the introduction of the second carbazolyl vinyl group, the main absorption peak of **B3** (672 nm) shows a bathochromic shift of 86 nm by comparison with **B2** due to the extension of π-conjugation. This is illustrated in Figure 5 in which the HOMO and LUMO densities are shown: in **B3** the HOMO is spread on both arms. As the LUMO are mostly localized on the BODIPY moiety, the π-conjugation extension leads to a reduced optical gap for **B3** compared to **B2**. Interestingly, the difference between the optical HOMO-LUMO in **B2** and **B3** is closed to the one measured in electrochemistry which amounted to 97

nm. In addition, there is a broad but weak absorption in the UV region ascribed to the S_0-S_n ($n \geq 2$) transitions of the BODIPY moiety for compounds **B2** and **B3**.[75] In summary, **B2** and **B3** can absorb longer-wavelength light, which suggest there use in light-harvesting systems.

The emission spectra of the two compounds were also recorded in CH_2Cl_2 solutions (Figure 4) and show perfect mirror symmetry with the absorption spectra with Stokes-shift in the range of 20-39 nm. The fluorescence emission maxima for compounds **B2** and **B3** are centered at 616 nm and 701 nm, respectively. The fluorescence quantum yields were also determined in CH_2Cl_2 (Table 3). The fluorescence quantum yields of **B2** and **B3** are 0.86 and 0.42, respectively. In addition, fluorescence lifetimes (τ) of these two BODIPY dyes were also measured, which show a single exponential decay with a lifetime of approximately 4 ns (Table 3).

Table 3. The photophysical properties of compounds **B2** and **B3** in DCM

Compound	λ_{abs} [nm]	λ_{em} [nm]	$\Delta\upsilon$ [cm^{-1}]	ε ($10^5 \cdot M^{-1} \cdot cm^{-1}$)	Φ_F	τ_F [ns]
B2	586	616	831	1.37	0.86	4.01
B3	672	701	616	1.48	0.42	3.92

Concentration: 1×10^{-5} M, Compound **B2** was excited at 520 nm, Compound **B3** was excited at 600 nm.

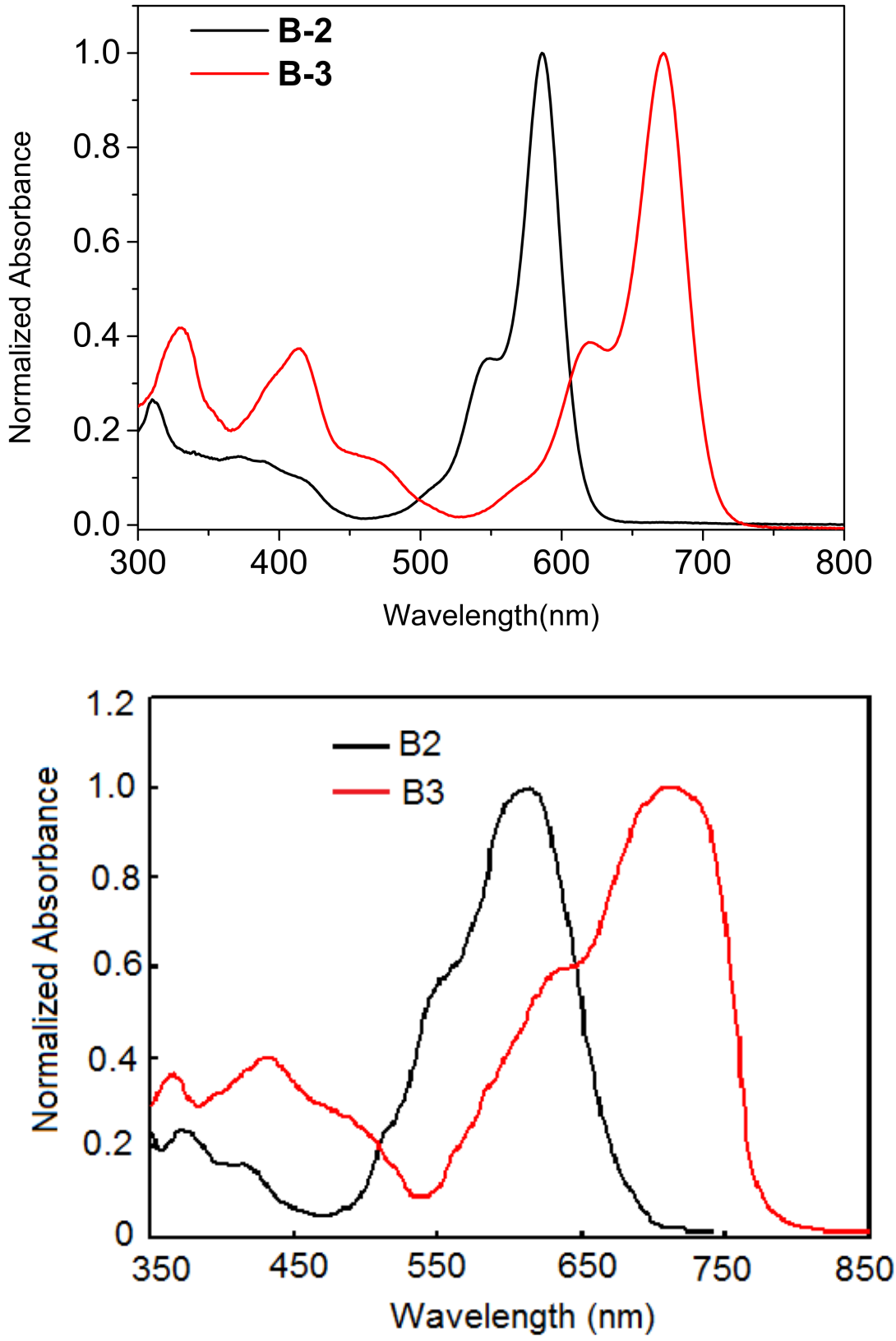

Figure 3. Normalized UV-vis spectra of compounds **B2** and **B3** in DCM (upper) solution and (bottom) film

The optical absorption spectra of **B2** and **B3** films are shown in Figure 3b. As compared to solution, the ICT band of thin film absorption is significantly red-shifted and also broaden; this may be attributed to the strong aggregation and molecular interaction in the solid state. The optical bandgap estimated from the onset absorption edge of the thin film absorption is about 1.78 eV and 1.58 eV for the **B2** and **B3**, respectively. The small optical bandgap for **B3** may be ascribed to its longer conjugation length as compared to **B2** due to the additional carbazole donor unit.

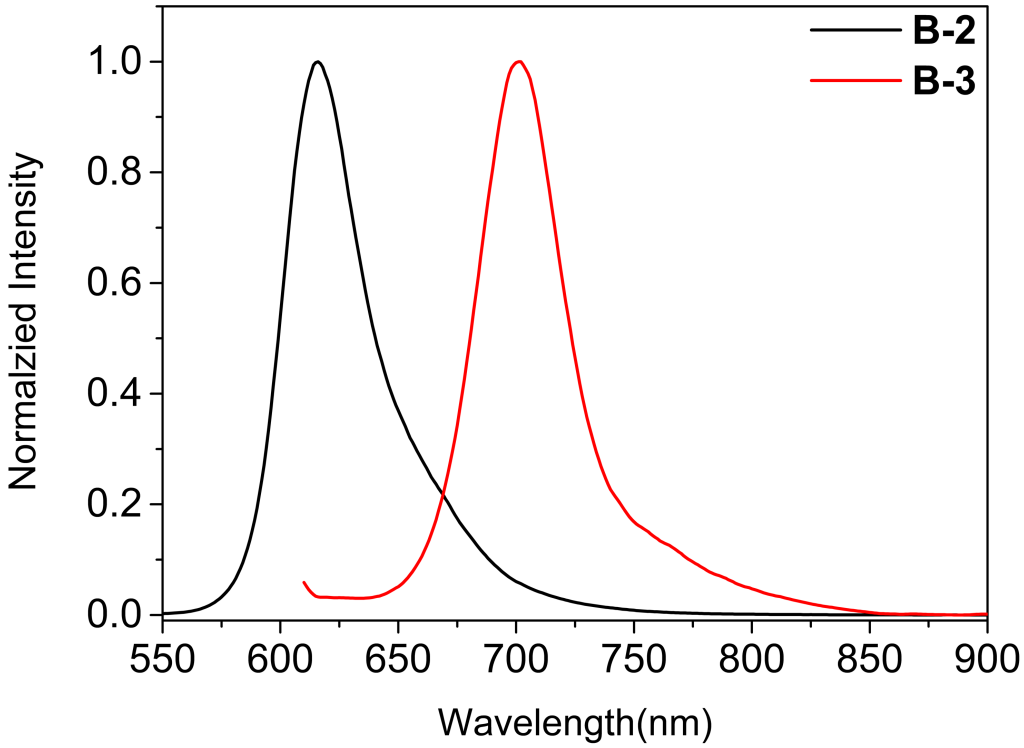

Figure 4. Emission spectra of compounds **B2** and **B3** in DCM

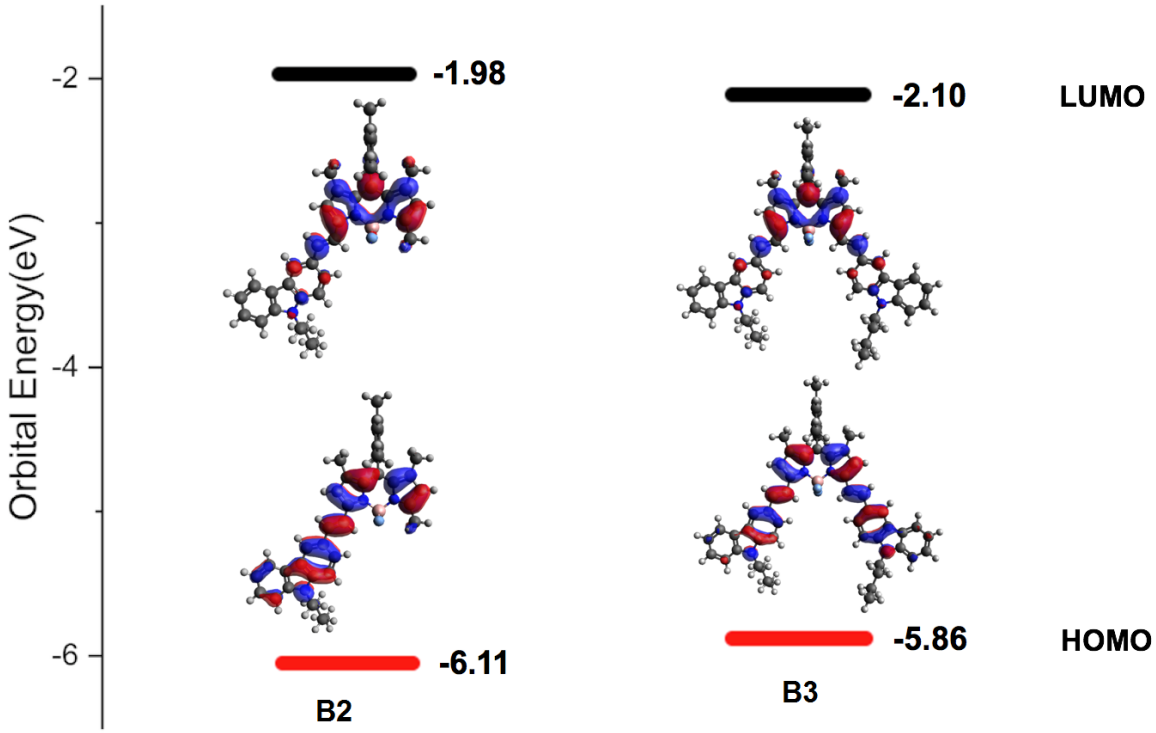

Figure 5. HOMO and LUMO energies (eV) and density (contour value=0.02, rendered with Avogadro [76, 77] for **B2** and **B3**.

3.4. Photovoltaic properties

BHJ OSCs with configuration glass/ITO/PEDOT:PSS/active layer/ PFN/Al were fabricated using **B2** and **B3** as electron donor material along with $PC_{71}BM$ as electron acceptor material. Since the relative content of the donor and acceptor in the active layer for OSCs is crucial for obtaining the mixed BHJ morphology and efficient exciton harvesting and formation of sufficient charge transport network.[20, 78] Initially, the photovoltaic performance of **B2** and **B3** were evaluated carefully *via* the variation of donor to acceptor weight *ratios* keeping the total concentration of 16 mg/mL using chloroform as solvent. We found that the device with 1:1.5 weight *ratio* showed the best Power Conversion Efficiency (PCE) about 3.21% and 3.59% for **B2**:$PC_{71}BM$ and **B3**:$PC_{71}BM$ active layers, respectively (Table 4). In order to further improve the PCE of the OSCs, we have adopted solvent vapor annealing (SVA) of the active layer

having D:A ratio of 1:1.5 with THF for 40 s and found that the PCE has been improved significantly. This is attributed to the improvement in the nanoscale morphology of the active layers.[79-81] The current-voltage characteristics of the OSCs based on optimized active layers are shown in Figure 6a and photovoltaic parameters are compiled in Table 4. The OSCs based on the **B2**:$PC_{71}BM$ and **B3**:$PC_{71}BM$ active layer after SVA treatment showed overall PCE of 6.41% (J_{sc} = 13.16 mA/cm^2, V_{oc} = 0.78 and FF =0.61) and 7.45% (J_{sc} = 16.18 mA/cm^2, V_{oc} = 0.71 V and FF = 0.65), respectively. Upon THF treatment, the Jsc and FF of the OSCs increase dramatically, and this may be attributed to the improvement in the nanoscale morphology of the active layer. However, the V_{oc} is reduced after SVA treatment which may be due to morphological changes at the contact interfaces and reduction in the quasi Fermi level gaps.[21]

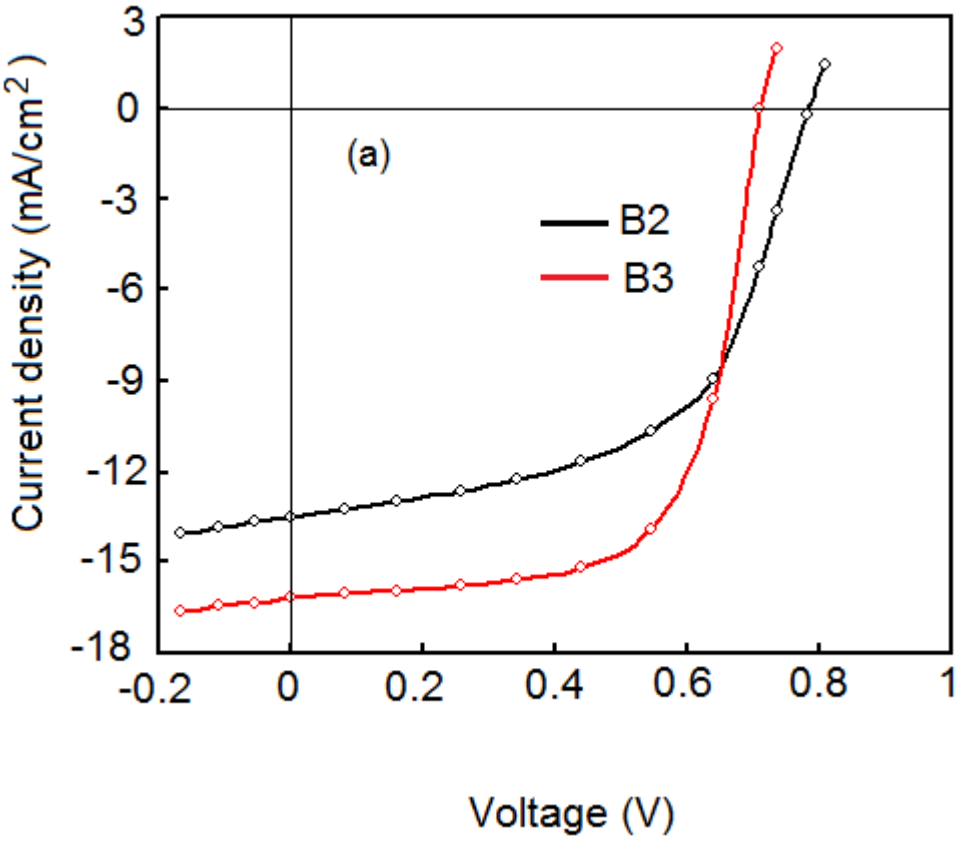

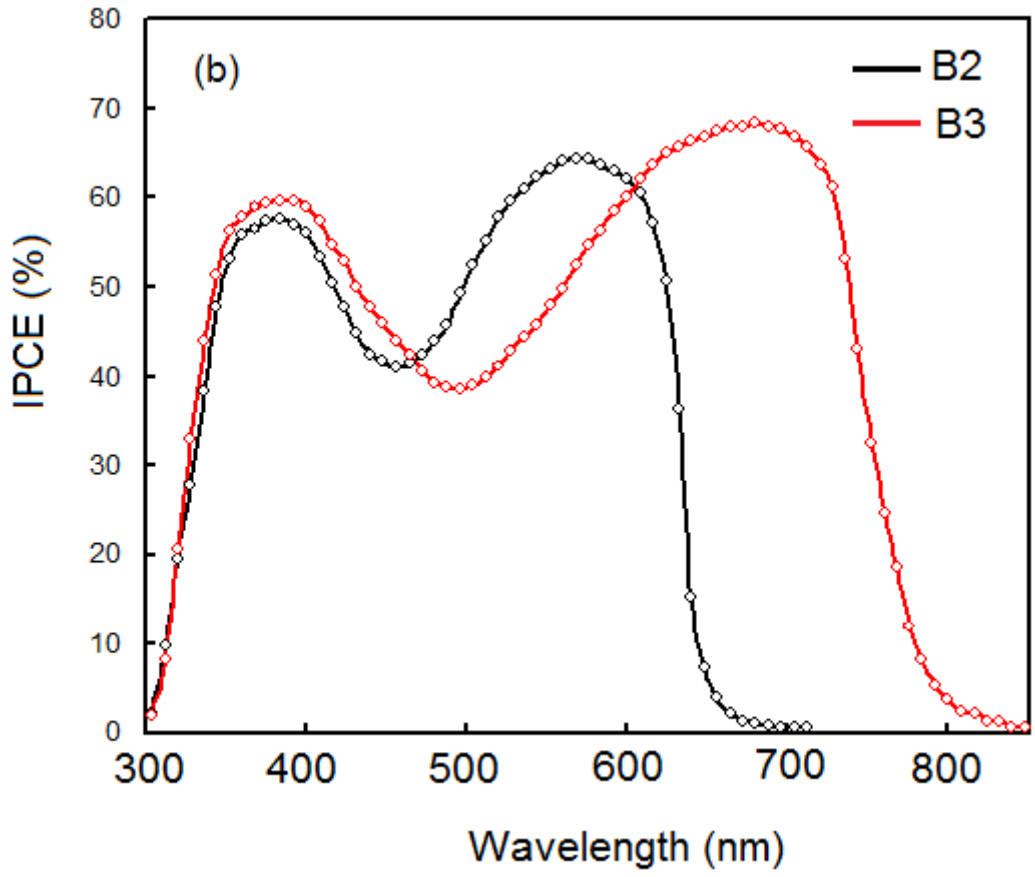

Figure 6. (a) Current-voltage characteristics under illumination and (b) IPCE spectra of the OSCs based on optimized **B2**:$PC_{71}BM$ and **B3**:$PC_{71}BM$ active layers

Table 4. Photovoltaic parameters of the OSCs based on **B2** and **B3** as donor and $PC_{71}BM$ as acceptor

Active layer	J_{sc} (mA/cm^2)	V_{oc} (V)	FF	PCE (%)	μ_h (cm^2/Vs)	μ_e (cm^2/Vs)	μ_e/μ_h
B2:$PC_{71}BM$ (as cast)	8.63	0.81	0.46	3.21 (3.08)[a]			
B3:$PC_{71}BM$ (as cast)	10.45	0.75	0.48	3.76 (3.63)[a]			
B2:$PC_{71}BM$ (SVA)	13.56	0.78	0.61	6.45 (6.32)[a]	8.89×10^{-5}	2.41×10^{-4}	2.71
B3:$PC_{71}BM$ (SVA)	16.24	0.71	0.66	7.61 (7.55)[a]	1.07×10^{-4}	2.47×10^{-4}	2.31

[a]Average of 8 devices

The V_{oc} value for the OSCs based on **B2** is higher than that for **B3** and this may be attributed to the deeper HOMO energy level of **B2**, since the V_{oc} is directly proportional to the energy offset between the HOMO of donor and LUMO of acceptor employed in the BHJ active layer of the OSCs. Since the HOMO and LUMO energy levels are about -6.05 eV and 4.10 eV, the $\Delta E_{HOMO\ (D)\text{-}LUMO\ (A)}$ offset for the **B2**:$PC_{71}BM$ and **B3**:$PC_{71}BM$ are equal to 1.065 eV and 0.89 eV, respectively, which is consistent with the trend in the values of V_{oc} in the OSCs. The value of J_{sc} is higher for **B3** than that for **B2**, and this may be related to the broader and lower bandgap of **B3** as compared to **B2**, leading to improved light harvesting capability of the **B3**:$PC_{71}BM$ active layer as compared to **B2**:$PC_{71}BM$. Moreover, the FF value for the **B3** based OSCs is also higher than **B2** counterparts, may be originated from the more balanced charge transport as discussed in the later part of the manuscript.

In order to get information about the higher value of J_{sc} for **B3** based OSCs as compared to **B2** counterpart, we have measured the incident photon to current conversion efficiency (IPCE) spectra of the OSCs and shown in Figure 6b. The IPCE spectra show two bands *i.e.* one in the wavelength region of 300-500 nm, which corresponds to the photocurrent generation due to the $PC_{71}BM$ and other beyond 500 nm corresponding to the photocurrent generation due to the donor (**B2** or **B3**), indicating that both donor and acceptor components in the BHJ active layer contribute to the photocurrent generation. As can be seen from the spectra, the IPCE spectrum for **B2** based is limited up to 650 nm whereas it is extended up to 790 nm for **B3** counterpart. The estimated values of J_{sc} from the IPCE spectra are about 13.39 mA/cm^2 and 16.12 mA/cm^2 for **B2** and **B3** based OSCs and are consistent with the values observed in J-V characteristics of the devices under illumination.

The charge transport in the active layer plays an important role for high values of FF and J_{sc}, therefore, we have measured the hole and electron mobilities in the active layers using the

hole only (ITO/PEDOT:PSS/active layer/Au) and electron only (ITO/Al/active layer/Al) devices, respectively. The hole and electron mobility values computed from the space charge limited current (SCLC) model are shown in Figure 7a and 7b for hole only and electron only devices, respectively. The hole mobility was found about 8.89×10^{-5} cm^2/Vs and 1.07×10^{-4} cm^2/Vs for **B2** and **B3**, respectively for optimized active layers. The electron mobility in the active layers are almost the same about 2.41×10^{-4} cm^2/Vs and 2.47×10^{-4} cm^2/Vs, respectively, leading to the electron to hole mobility *ratio* about 3.65 and 2.59, for the active layers based on **B2** and **B3**, respectively. The reduction of electron to hole mobility *ratio* for **B2** based device contributes to the enhancement in the charge transport within the active layer, hence leading to the higher values of J_{sc} and FF.

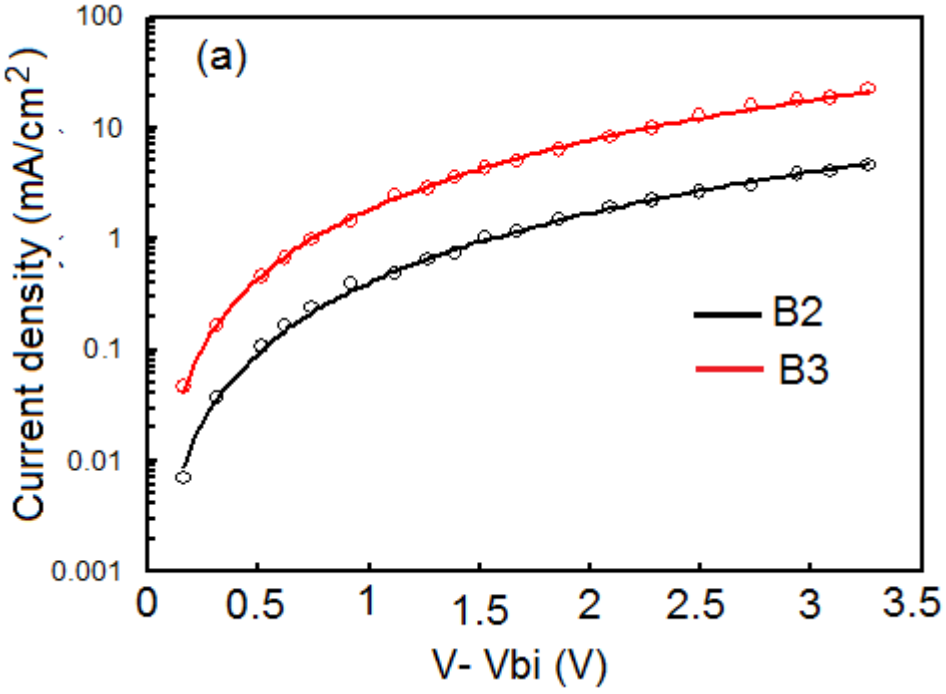

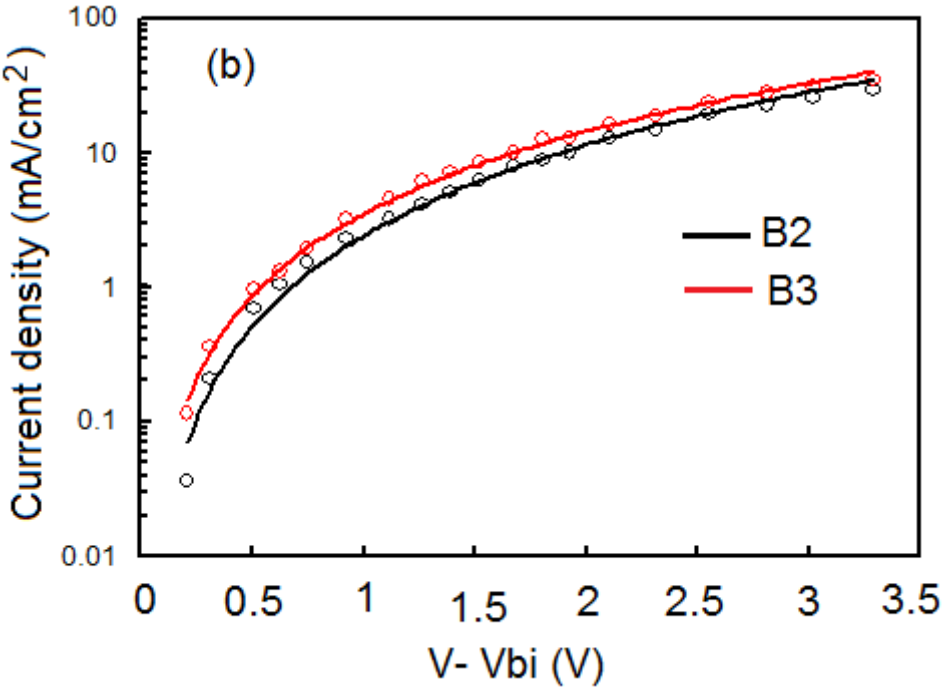

Figure 7. Dark current-voltage characteristics of the (a) hole and (b) electron only devices based on optimized **B2**:$PC_{71}BM$ and **B3**:$PC_{71}BM$ active layers (the solid lines are SCLC fitting)

In order to get information about the difference in the charge generation, recombination and extraction process, in the OSCs based on **B2** and **B3**, the variation of photocurrent density (J_{ph}) with effective voltage (V_{eff}) was analyzed and is shown in Figure 8. J_{ph} is described as $J_{ph} = J_L - J_d$, where J_L and J_D are the current densities under illumination and in the dark, respectively. The V_{eff} is defined as $V_{eff} = V_o - V_a$, where V_o is the voltage at which J_{ph} is zero and V_a is the applied voltage. As can be seen from this figure, in both devices, Jph increases linearly with V_{eff} at low voltages and tends to saturate at the V_{eff} = 0.92 V and 0.64 V for **B2** and **B3**, respectively and completely saturate to saturation photocurrent (J_{phsat}) at high value of V_{eff}, indicating that all the photogenerated excitons are dissociated into free charge carriers and efficiently collected by the electrodes. The exciton dissociation efficiency (P_{diss}) and charge collection efficiency (P_{coll}) were estimated as J_{ph}/J_{Phsat} under short circuit and maximum power point conditions, respectively.[82, 83] The values of P_{diss}/P_{coll} for the devices

based on the **B2** and **B3** are about 0.907/0.642 and 0.948/0.723, respectively. These observations support that exciton dissociation and collection is more efficient for **B3** based OSCs than that for **B2** and may be the origin for high values of J_{sc} and FF for the **B3** based OSCs. Generally, at high value of $V_{eff,}$ all the photogenerated excitons are dissociated into free charge carriers and J_{phsat} mainly depends on the exciton generation rate (G_{max}) which is described as $J_{phsat}= qLG_{max}$, where q is the electronic charge and L is the thickness of the active layer. The values of G_{max} of the optimized OSCs are about 1.03×10^{28} $m^{-3}s^{-1}$ and 1.12×10^{28} $m^{-3}s^{-1}$ for **B2** and **B3**, respectively. The higher value of G_{max} for **B3** based as compared to **B2** counterpart indicates that more excitons are generated in the **B3**:$PC_{71}BM$ active layer (particularly in **B3**) due to the broader absorption spectra of **B3**.

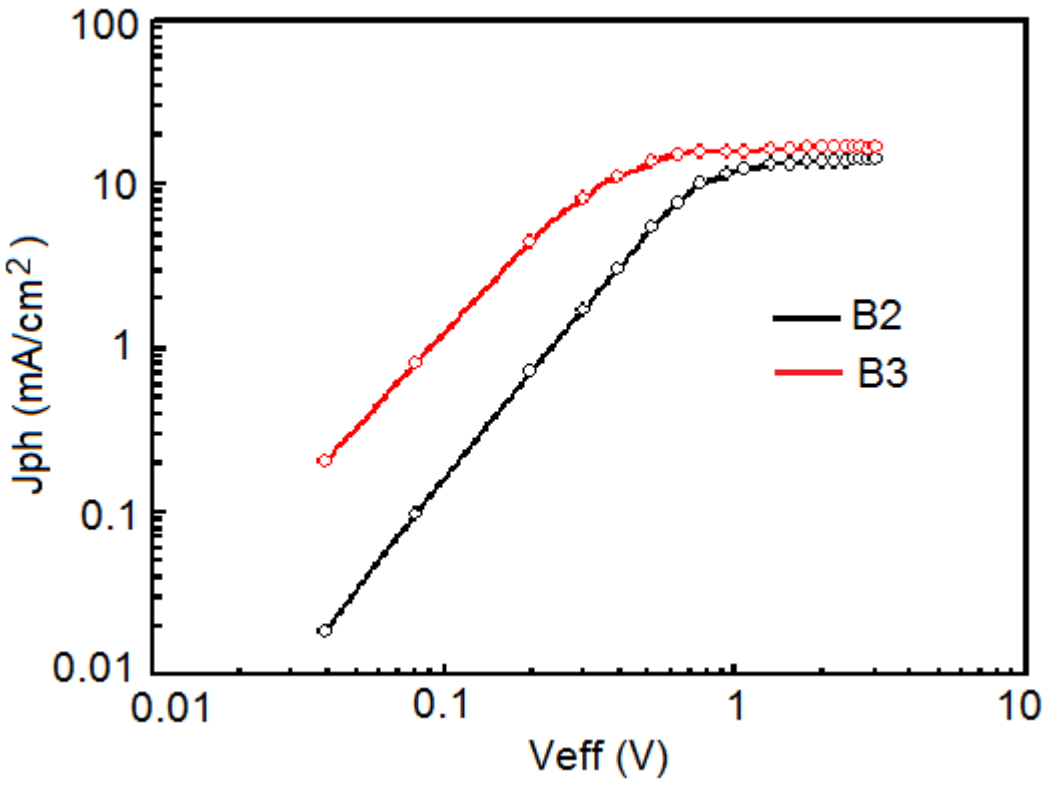

Figure 8. Variation of photocurrent density (J_{ph}) with effective voltage (V_{eff}) for the OSCs based on optimized **B2**:$PC_{71}BM$ and **B3**:$PC_{71}BM$ active layers

In order to get more information about the difference in the recombination processes in the OSCs based on **B2** and **B3**, we have measured the variation of J_{sc} with illumination intensity $(P_{in})^{84-86}$ as shown in Figure 9a, which if described as $J_{sc} \propto (P_{in})^{\alpha}$, where α is the exponent that describe the degree of recombination. The bimolecular recombination is negligible when the value of α is unity, whereas when α is less than unity there is a competition between the recombination and charge recombination. The value of α for the device based on **B2** and **B3** are about 0.91 and 0.94, respectively, indicating the bimolecular recombination is less for **B3** based device and leading to the high value of FF.

The variation of V_{oc} with P_{in} for the OSCs are shown in Figure 9b. The V_{oc} is proportional to S [ln (P_{in})], where S is the slope extracted from the linear fit of V_{oc} with ln (P_{in}). When S is equal to 1 kT/q, the bimolecular recombination is the dominant mechanism whereas a larger value of S than 1kT/q indicates that the trap-assisted recombination or germinating recombination may be dominating in the devices. The values of S estimated from the Figure 9b are 1.56 kT/q and 1.38 kT/q for **B2** and **B3** based devices, indicating that the trap-assisted recombination is less for the **B3** based OSCs. Therefore, the higher values of J_{sc} and FF for the **B3** based OSCs can be due to the high exciton dissociation, weak bimolecular recombination and trap-assisted recombination, which are related to the molecular packing crystalline nature of the active layer.

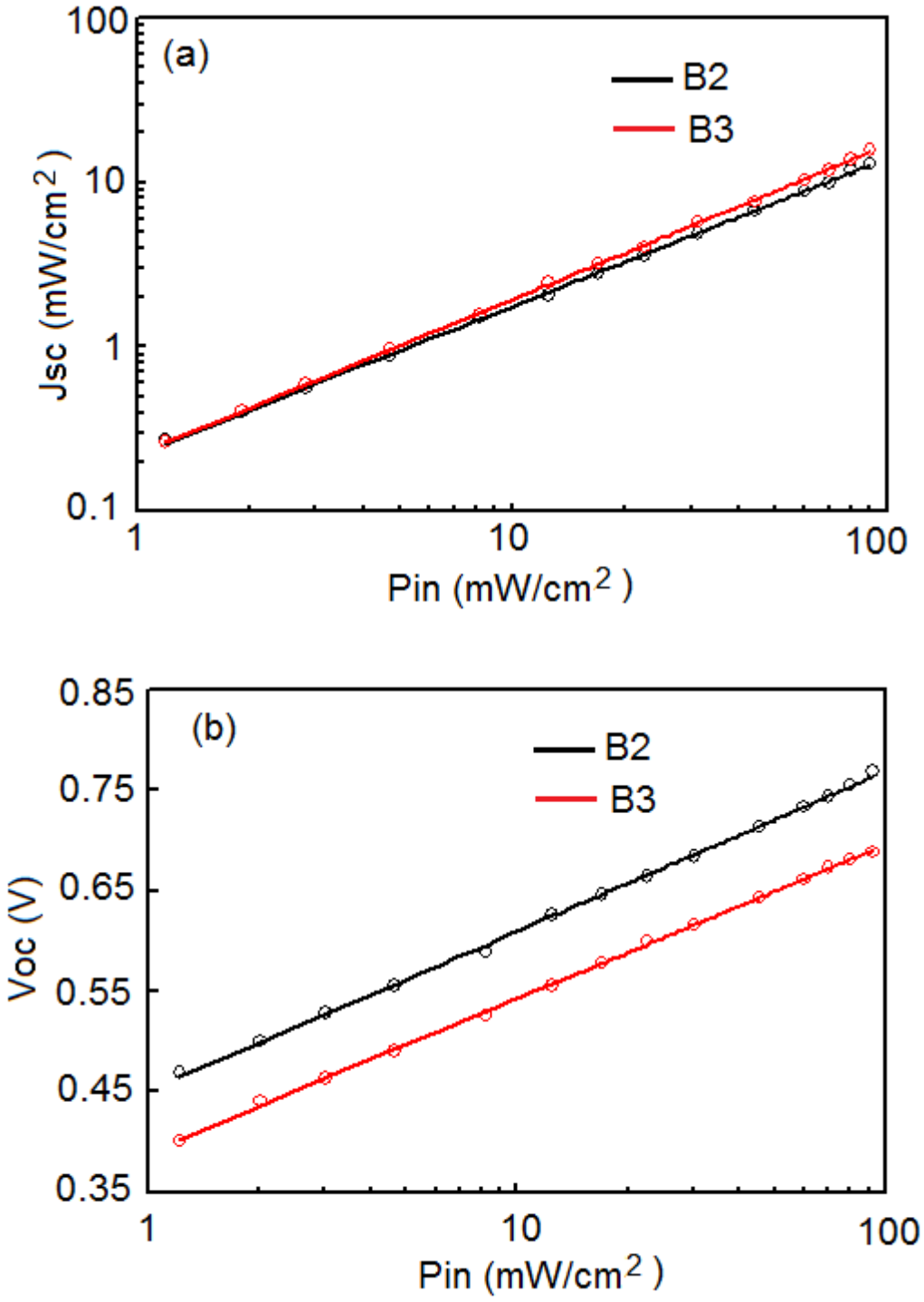

Figure 9. Variation of (a) J_{sc} and (b) V_{oc} with illumination intensity (P_{in}) for the OSCs based on optimized active layers based on **B2** and **B3**

In order to get the information about the crystallinity and the molecular ordering of the optimized active layer based on **B2**:$PC_{71}BM$ and **B3**:$PC_{71}BM$ as well as for the pristine **B2** and **B3**, the X-ray diffraction measurements were performed and shown in Figure 10 for

optimized blends and Figure S9 (ESI) for pristine films. The pristine **B2** and **B3** film show same strong (100) diffraction peak at 2θ = 5.24° and different (010) diffraction peaks at 2θ = 22.98° and 23.30°, for **B2** and **B3**, respectively. When blended with $PC_{71}BM$, both the active layers show a strong (100) diffraction peak at 2θ = 5.06°, which corresponds to the lamellar distance of 1.88 nm. However, the (010) diffraction peaks for the **B2**:$PC_{71}BM$ and **B3**:$PC_{71}BM$ are observed at 2θ = 22.74° and 23.08°, respectively, corresponding to the π-π stacking distances of 0.408 nm and 0.389 nm, respectively. In addition of these peaks, a weak diffraction peak around 2θ = 18° is also observed in both the thin films, which corresponds to $PC_{71}BM$.[87] Moreover, both the diffraction peaks are stronger for **B3** based thin film as compared to **B2** indicating that the degree of crystallinity is more for former than later. The enhanced crystalline nature and reduced π-π stacking distance for the **B3**:$PC_{71}BM$ active layer may induced the better nanoscale phase separation and beneficial for charge transport and collection. These observations may be the origin for higher FF and greater PCE of OSC based on **B3**:$PC_{71}BM$ active layer.

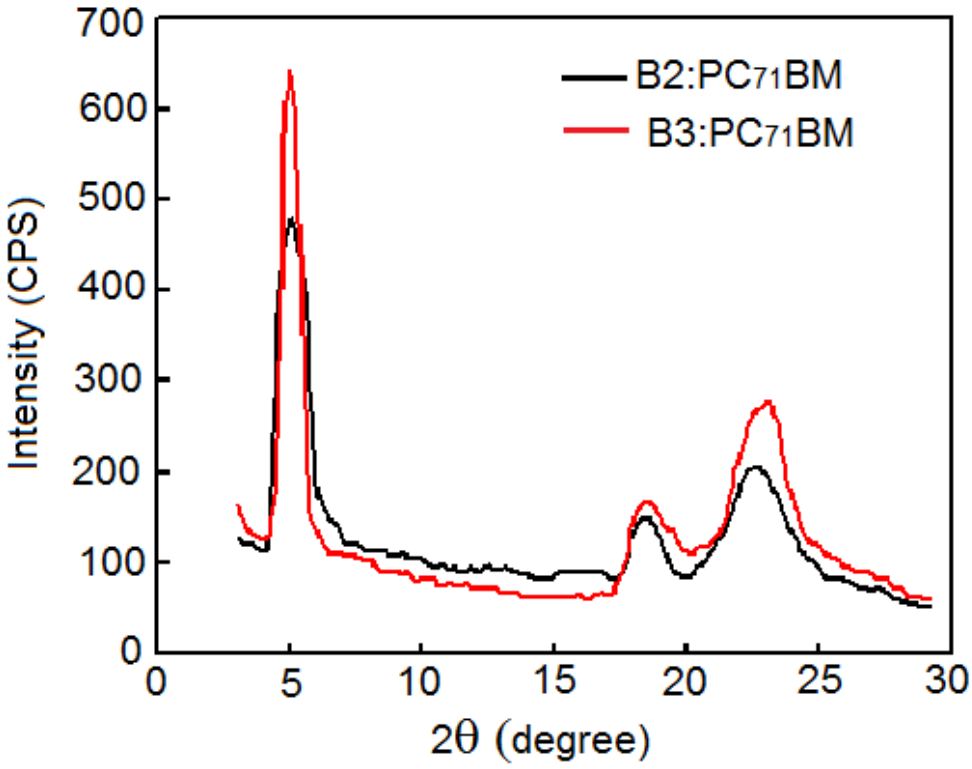

Figure 10. X-ray diffraction (XRD) patterns of the optimized **B2**:$PC_{71}BM$ and **B3**:$PC_{71}BM$ thin films

We have also investigated the morphology of the optimized **B2**:$PC_{71}BM$ and **B3**:$PC_{71}B$ active layers by recording the Transmission Electron Microscopy (TEM) images as shown in Figure 11. It can be seen from these images that the donor (**B2** or **B3**) and acceptor formed a bi-continuous interpenetrating network in both blend films, which assurances effective exciton dissociation and charge transfer channels. The **B3**:$PC_{71}BM$ blend forms better phase separation than that for **B2**:$PC_{71}BM$ indicating more effective charge transfer in **B3**:$PC_{71}BM$, which is consistent with the high value of FF for **B3**:$PC_{71}BM$ based OSCs.

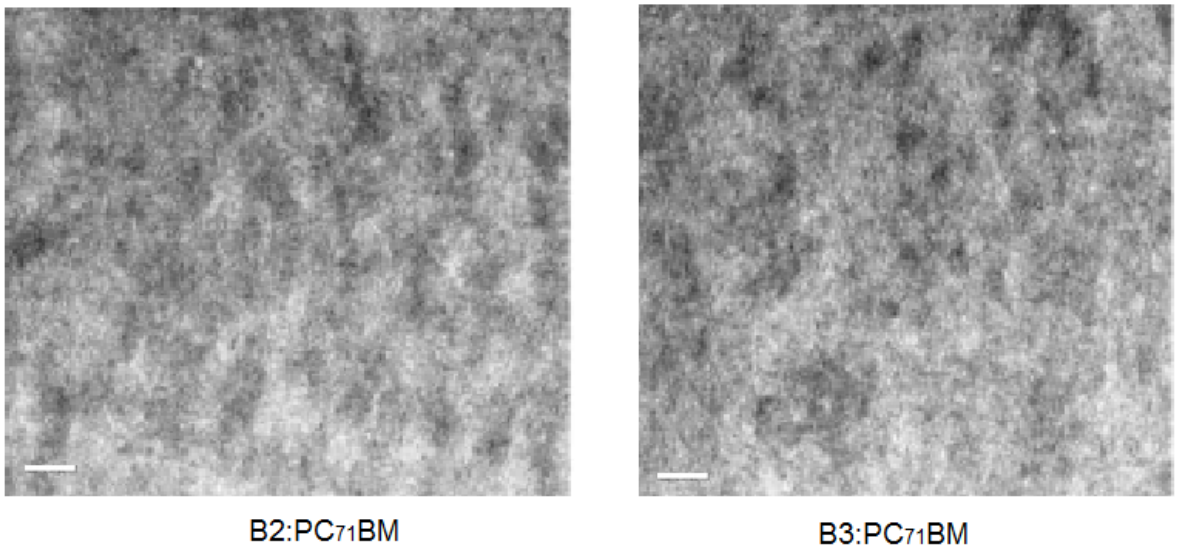

Figure 11. TEM images optimized **B2**:$PC_{71}BM$ and **B3**:$PC_{71}BM$ with bar scale 200 nm

4. Conclusions

Two BODIPY with one (**B2**) and two carbazole (**B3**) units were designed and synthesized. Their optical and electrochemical properties were investigated for their potential application as donor materials for the solution processed bulk heterojunction organic solar cells employing PCBM as electron acceptors. The optimized **B2**:$PC_{71}BM$ and **B3**:$PC_{71}BM$ based OSCs showed overall PCE of 6.41% and 7.47%, respectively. The higher PCE of **B3**:$PC_{71}BM$ than **B2**:$PC_{71}BM$ is mainly due to the enhanced values of J_{sc} and FF and may be related to the better charge transport and exciton dissociation. The optical absorption spectra and frontier energy levels of **B2** and **B3** may also be suitable for non-fullerene acceptors since these two small molecules showed complementary absorption spectra and can be employed for ternary OSCs. We are working in this direction and expecting to achieve higher PCE.

ORCID

Charles H. Devillers: 0000-0001-9078-7035

Paul Fleurat-Lessard: 0000-0003-3114-2522

Claude P. Gros: 0000-0002-6966-947X

Ganesh D. Sharma: 0000-0002-1717-0116

Hai-Jun Xu: 0000-0002-8721-3310

Author Contributions

The manuscript was written through contributions of all authors. All authors have given approval to the final version of the manuscript.

Acknowledgments

Support was provided by the CNRS (UMR 6302), the *Université Bourgogne Franche-Comté*, the *Conseil Régional de Bourgogne* through the *Plan d'Actions Régional pour l'Innovation* (PARI II CDEA) and the European Union through the PO FEDER-FSE Bourgogne 2014/2020 programs. National Key R&D Program of China (2016YFD0600804), Natural Scientific Foundation of Jiangsu Province, P. R. China (No. BK20160922), National Natural Scientific Foundation of China (No. 21301092). C. H. D. thanks the *Agence Nationale de la Recherche* for funding (ANR-15-CE29-0018-01). The french authors thank the *Plateforme d'Analyse Chimique et de Synthèse Moléculaire de l'Université de Bourgogne* (PACSMUB, http://www.wpcm.fr) for access to analytical and spectroscopy instrumentation. G. D. S. and G. G. thanks to Department of Science and Technology, Government of India, New Delhi for financial support. Calculations were performed using HPC resources from DNUM CCUB (Centre de Calcul de l'Université de Bourgogne).

Conflict of Interest

The authors declare no conflict of interest.

Keywords

Green and blue-BODIPY, electrochemistry, bulk heterojunction, power conversion efficiency

References

1. J. Roncali, *Acc. Chem. Res.*, 2009, **42**, 1719-1730.
2. Y. Kubota, K. Kimura, J. Jin, K. Manseki, K. Funabiki and M. Matsui, *New J. Chem.*, 2019, **43**, 1156-1165.
3. L. Bucher, N. Desbois, E. N. Koukaras, C. H. Devillers, S. Biswas, G. D. Sharma and C. P. Gros, *J. Mater. Chem. A*, 2018, **6**, 8449-8461.
4. Y. Cai, L. Huo and Y. Sun, *Adv. Mater.*, 2017, **29**, 1605437.
5. J. Huang, H. Wang, K. Yan, X. Zhang, H. Chen, C. Z. Li and J. Yu, *Adv Mater*, 2017, **29**, 1606729.
6. H. Yao, L. Ye, H. Zhang, S. Li, S. Zhang and J. Hou, *Chem. Rev.*, 2016, **116**, 7397-7457.
7. A. Bessette and G. S. Hanan, *Chem. Soc. Rev.*, 2014, **43**, 3342-3405.
8. N. K. Elumalai and A. Uddin, *Energy & Environmental Science*, 2016, **9**, 391-410.
9. G. Thumuganti, V. Gupta and S. P. Singh, *New J. Chem.*, 2019, **43**, 8735-8740.
10. Z.-W. Zhao, Q.-Q. Pan, Y.-C. Duan, Y. Wu, Y. Geng, S.-X. Wu and Z.-M. Su, *J. Phys. Chem. C*, 2019, **123**, 6407-6415.
11. B. Qiu, L. Xue, Y. Yang, H. Bin, Y. Zhang, C. Zhang, M. Xiao, K. Park, W. Morrison, Z.-G. Zhang and Y. Li, *Chem. Mater.*, 2017, **29**, 7543-7553.
12. B. Kan, M. Li, Q. Zhang, F. Liu, X. Wan, Y. Wang, W. Ni, G. Long, X. Yang, H. Feng, Y. Zuo, M. Zhang, F. Huang, Y. Cao, T. P. Russell and Y. Chen, *J. Am. Chem. Soc.*, 2015, **137**, 3886-3893.
13. S. Li, L. Ye, W. Zhao, S. Zhang, S. Mukherjee, H. Ade and J. Hou, *Adv. Mater.*, 2016, **28**, 9423-9429.

14. F. Zhao, S. Dai, Y. Wu, Q. Zhang, J. Wang, L. Jiang, Q. Ling, Z. Wei, W. Ma, W. You, C. Wang and X. Zhan, *Adv. Mater.*, 2017, **29**, 1700144.
15. W. Zhao, S. Li, H. Yao, S. Zhang, Y. Zhang, B. Yang and J. Hou, *J. Am. Chem. Soc.*, 2017, **139**, 7148-7151.
16. X. Che, Y. Li, Y. Qu and S. R. Forrest, *Nature Energy*, 2018, **3**, 422-427.
17. G. D. Sharma, S. A. Siddiqui, A. Nikiforou, G. E. Zervaki, I. Georgakaki, K. Ladomenou and A. G. Coutsolelos, *J. Mater. Chem. C*, 2015, **3**, 6209-6217.
18. S. D. Collins, N. A. Ran, M. C. Heiber and T.-Q. Nguyen, *Adv. Energy Mater.*, 2017, **7**, 1602242.
19. A. Mishra and P. Bauerle, *Angew. Chem. Int. Ed. Engl.*, 2012, **51**, 2020-2067.
20. Y. Lin, Y. Li and X. Zhan, *Chem. Soc. Rev.*, 2012, **41**, 4245-4272.
21. B. Kan, Q. Zhang, M. Li, X. Wan, W. Ni, G. Long, Y. Wang, X. Yang, H. Feng and Y. Chen, *J. Am. Chem. Soc.*, 2014, **136**, 15529-15532.
22. Y. Liu, C. C. Chen, Z. Hong, J. Gao, Y. M. Yang, H. Zhou, L. Dou, G. Li and Y. Yang, *Sci Rep*, 2013, **3**, 3356.
23. L. Meng, Y. Zhang, X. Wan, C. Li, X. Zhang, Y. Wang, X. Ke, Z. Xiao, L. Ding, R. Xia, H. L. Yip, Y. Cao and Y. Chen, *Science*, 2018, **361**, 1094-1098.
24. L. Lu, T. Zheng, Q. Wu, A. M. Schneider, D. Zhao and L. Yu, *Chem. Rev.*, 2015, **115**, 12666-12731.
25. M. C. Scharber, D. Mühlbacher, M. Koppe, P. Denk, C. Waldauf, A. J. Heeger and C. J. Brabec, *Adv. Mater.*, 2006, **18**, 789-794.
26. P. Cheng and X. Zhan, *Chem. Soc. Rev.*, 2016, **45**, 2544-2582.
27. J. Tao, D. Sun, L. Sun, Z. Li, B. Fu, J. Liu, L. Zhang, S. Wang, Y. Fang and H. Xu, *Dyes and Pigments*, 2019, **168**, 166-174.

28. R. R. Petrov, L. Knight, S.-R. Chen, J. Wager-Miller, S. W. McDaniel, F. Diaz, F. Barth, H.-L. Pan, K. Mackie, C. N. Cavasotto and P. Diaz, *Eur. J. Med. Chem.*, 2013, **69**, 881-907.
29. M. J. Frisch, G. W. Trucks, H. B. Schlegel, G. E. Scuseria, M. A. Robb, J. R. Cheeseman, G. Scalmani, V. Barone, G. A. Petersson, H. Nakatsuji, X. Li, M. Caricato, A. V. Marenich, J. Bloino, B. G. Janesko, R. Gomperts, B. Mennucci, H. P. Hratchian, J. V. Ortiz, A. F. Izmaylov, J. L. Sonnenberg, Williams, F. Ding, F. Lipparini, F. Egidi, J. Goings, B. Peng, A. Petrone, T. Henderson, D. Ranasinghe, V. G. Zakrzewski, J. Gao, N. Rega, G. Zheng, W. Liang, M. Hada, M. Ehara, K. Toyota, R. Fukuda, J. Hasegawa, M. Ishida, T. Nakajima, Y. Honda, O. Kitao, H. Nakai, T. Vreven, K. Throssell, J. A. Montgomery Jr., J. E. Peralta, F. Ogliaro, M. J. Bearpark, J. J. Heyd, E. N. Brothers, K. N. Kudin, V. N. Staroverov, T. A. Keith, R. Kobayashi, J. Normand, K. Raghavachari, A. P. Rendell, J. C. Burant, S. S. Iyengar, J. Tomasi, M. Cossi, J. M. Millam, M. Klene, C. Adamo, R. Cammi, J. W. Ochterski, R. L. Martin, K. Morokuma, O. Farkas, J. B. Foresman and D. J. Fox, *Journal*, 2016.
30. Y. Zhao and D. G. Truhlar, *Theor. Chem. Acc.*, 2007, **120**, 215-241.
31. A. Loudet and K. Burgess, *Chem. Rev.*, 2007, **107**, 4891-4932.
32. X. Kong, L. Di, Y. Fan, Z. Zhou, X. Feng, L. Gai, J. Tian and H. Lu, *Chem. Comm.*, 2019, **55**, 11567-11570.
33. G. Ulrich, R. Ziessel and A. Harriman, *Angew. Chem. Int. Ed. Engl.*, 2008, **47**, 1184-1201.
34. X.-Y. Zhu, H. Wu, X.-F. Guo and H. Wang, *Dyes and Pigments*, 2019, **165**, 400-407.
35. J. Yang, Y. Fan, F. Cai, X. Xu, B. Fu, S. Wang, Z. Shen, J. Tian and H. Xu, *Dyes and Pigments*, 2019, **164**, 105-111.

36. B. Kucukoz, G. Sevinc, E. Yildiz, A. Karatay, F. Zhong, H. Yilmaz, Y. Tutel, M. Hayvali, J. Zhao and H. G. Yaglioglu, *Phys. Chem. Chem. Phys.*, 2016, **18**, 13546-13553.
37. X. Zheng, W. Du, L. Gai, X. Xiao, Z. Li, L. Xu, Y. Tian, M. Kira and H. Lu, *Chem. Comm.*, 2018, **54**, 8834-8837.
38. A. Turksoy, D. Yildiz and E. U. Akkaya, *Coord. Chem. Rev.*, 2019, **379**, 47-64.
39. S. Baysec, A. Minotto, P. Klein, S. Poddi, A. Zampetti, S. Allard, F. Cacialli and U. Scherf, *Sci. China Chem.*, 2018, **61**, 932-939.
40. A. Zampetti, A. Minotto, B. M. Squeo, V. G. Gregoriou, S. Allard, U. Scherf, C. L. Chochos and F. Cacialli, *Sci. Rep.*, 2017, **7**, 1611.
41. H. Klfout, A. Stewart, M. Elkhalifa and H. He, *ACS Appl. Mater. Interfaces*, 2017, **9**, 39873-39889.
42. T. Hua, K. Zhang, Z.-S. Huang, L. Wang, H. Tang, H. Meier and D. Cao, *J. Mater. Chem. C*, 2019, **7**, 10379-10388.
43. C. Bonnier, D. D. Machin, O. Abdi and B. D. Koivisto, *Org. Biomol. Chem.*, 2013, **11**, 3756-3760.
44. H. Lu, J. Mack, Y. Yang and Z. Shen, *Chem. Soc. Rev.*, 2014, **43**, 4778-4823.
45. G. Tarafdar, U. K. Pandey, S. Sengupta and P. C. Ramamurthy, *Solar Energy*, 2019, **186**, 215-224.
46. J. Zhao, K. Xu, W. Yang, Z. Wang and F. Zhong, *Chem. Soc. Rev.*, 2015, **44**, 8904-8939.
47. Z. Lu, M. Liang, P. Dai, K. Miao, C. Zhang, Z. Sun and S. Xue, *J. Phys. Chem. C*, 2016, **120**, 25657-25667.
48. R. Ziessel, C. Goze, G. Ulrich, M. Cesario, P. Retailleau, A. Harriman and J. P. Rostron, *Chem. Eur. J.*, 2005, **11**, 7366-7378.
49. J. Zhang, F. Lu, S. Qi, Y. Zhao, K. Wang, B. Zhang and Y. Feng, *Dyes and Pigments*, 2016, **128**, 296-303.

50. M. D. Yilmaz, O. A. Bozdemir and E. U. Akkaya, *Org. Lett.*, 2006, **8**, 2871-2873.
51. T. Rousseau, A. Cravino, T. Bura, G. Ulrich, R. Ziessel and J. Roncali, *Chem. Commun.*, 2009, DOI: Doi 10.1039/B822770e, 1673-1675.
52. S. Y. Leblebici, L. Catane, D. E. Barclay, T. Olson, T. L. Chen and B. Ma, *ACS Appl. Mater. Interfaces*, 2011, **3**, 4469-4474.
53. T. Bura, N. Leclerc, S. Fall, P. Leveque, T. Heiser, P. Retailleau, S. Rihn, A. Mirloup and R. Ziessel, *J. Am. Chem. Soc.*, 2012, **134**, 17404-17407.
54. H. Y. Lin, W. C. Huang, Y. C. Chen, H. H. Chou, C. Y. Hsu, J. T. Lin and H. W. Lin, *Chem. Commun.*, 2012, **48**, 8913-8915.
55. W. Liu, A. Tang, J. Chen, Y. Wu, C. Zhan and J. Yao, *ACS Appl. Mater. Interfaces*, 2014, **6**, 22496-22505.
56. A. Mirloup, N. Leclerc, S. Rihn, T. Bura, R. Bechara, A. Hébraud, P. Lévêque, T. Heiser and R. Ziessel, *New J. Chem.*, 2014, **38**, 3644-3653.
57. A. Sutter, P. Retailleau, W.-C. Huang, H.-W. Lin and R. Ziessel, *New J. Chem.*, 2014, **38**, 1701-1710.
58. T. Jadhav, R. Misra, S. Biswas and G. D. Sharma, *Phys. Chem. Chem. Phys.*, 2015, **17**, 26580-26588.
59. I. Bulut, Q. Huaulme, A. Mirloup, P. Chavez, S. Fall, A. Hebraud, S. Mery, B. Heinrich, T. Heiser, P. Leveque and N. Leclerc, *ChemSusChem*, 2017, **10**, 1878-1882.
60. J. Liao, Y. Xu, H. Zhao, Q. Zong and Y. Fang, *Org. Electronics*, 2017, **49**, 321-333.
61. R. Srinivasa Rao, A. Bagui, G. Hanumantha Rao, V. Gupta and S. P. Singh, *Chem. Commun.*, 2017, **53**, 6953-6956.
62. T.-y. Li, J. Benduhn, Y. Li, F. Jaiser, D. Spoltore, O. Zeika, Z. Ma, D. Neher, K. Vandewal and K. Leo, *J. Mater. Chem. A*, 2018, **6**, 18583-18591.

63. J. Liao, H. Zhao, Y. Xu, Z. Cai, Z. Peng, W. Zhang, W. Zhou, B. Li, Q. Zong and X. Yang, *Dyes and Pigments*, 2016, **128**, 131-140.

64. A. Aguiar, J. Farinhas, W. da Silva, M. E. Ghica, C. M. A. Brett, J. Morgado and A. J. F. N. Sobral, *Dyes and Pigments*, 2019, **168**, 103-110.

65. N. Blouin, A. Michaud, D. Gendron, S. Wakim, E. Blair, R. Neagu-Plesu, M. Belletete, G. Durocher, Y. Tao and M. Leclerc, *J. Am. Chem .Soc.*, 2008, **130**, 732-742.

66. R. Qin, W. Li, C. Li, C. Du, C. Veit, H. F. Schleiermacher, M. Andersson, Z. Bo, Z. Liu, O. Inganas, U. Wuerfel and F. Zhang, *J. Am. Chem. Soc.*, 2009, **131**, 14612-14613.

67. D. Zhang, V. Martin, I. Garcia-Moreno, A. Costela, M. E. Perez-Ojeda and Y. Xiao, *Phys. Chem. Chem. Phys.*, 2011, **13**, 13026-13033.

68. X. Zhang, Y. Zhang, L. Chen and Y. Xiao, *RSC Advances*, 2015, **5**, 32283-32289.

69. C. M. Cardona, W. Li, A. E. Kaifer, D. Stockdale and G. C. Bazan, *Adv. Mater.* , 2011, **23**, 2367-2371.

70. H. Wang, Q. Yue, T. Nakagawa, A. Zieleniewska, H. Okada, K. Ogumi, H. Ueno, D. M. Guldi, X. Zhu and Y. Matsuo, *J. Mater. Chem. A* 2019, **7**, 4072-4083.

71. A. B. Nepomnyashchii, M. Bröring, J. Ahrens and A. J. Bard, *J. Am. Chem. Soc.*, 2011, **133**, 8633-8645.

72. A. A. Bakulin, A. Rao, V. G. Pavelyev, P. H. van Loosdrecht, M. S. Pshenichnikov, D. Niedzialek, J. Cornil, D. Beljonne and R. H. Friend, *Science*, 2012, **335**, 1340-1344.

73. Y. Sun, Z. Qu, Z. Zhou, L. Gai and H. Lu, *Org. Biomol. Chem.*, 2019, **17**, 3617-3622.

74. J. Xu, L. Zhu, Q. Wang, L. Zeng, X. Hu, B. Fu and Z. Sun, *Tetrahedron*, 2014, **2014 v.70**, pp. 5800-5805.

75. S. Wang, H. Lu, Y. Wu, X. Xiao, Z. Li, M. Kira and Z. Shen, *Chem - An Asian J* . 2017, **12**, 561–567.

76. *Avogadro*: an open-source molecular builder and visualization tool. Version 1.2.0. http://avogadro.cc/

77. M. D. Hanwell, D. E. Curtis, D. C. Lonie, T. Vandermeersch, E. Zurek and G. R. Hutchison, *J Cheminform*, 2012, **4**, 17.

78. G. J. Hedley, A. Ruseckas and I. D. Samuel, *Chem. Rev.*, 2017, **117**, 796-837.

79. K. Sun, Z. Xiao, E. Hanssen, M. F. G. Klein, H. H. Dam, M. Pfaff, D. Gerthsen, W. W. H. Wong and D. J. Jones, *J. Mater. Chem. A*, 2014, **2**, 9048-9054.

80. M. Li, F. Liu, X. Wan, W. Ni, B. Kan, H. Feng, Q. Zhang, X. Yang, Y. Wang, Y. Zhang, Y. Shen, T. P. Russell and Y. Chen, *Adv. Mater.*, 2015, **27**, 6296-6302.

81. J. Min, X. Jiao, I. Ata, A. Osvet, T. Ameri, P. Bäuerle, H. Ade and C. J. Brabec, *Adv. Energy Mater.*, 2016, **6**, 1502579.

82. Z. He, C. Zhong, X. Huang, W. Y. Wong, H. Wu, L. Chen, S. Su and Y. Cao, *Adv. Mater.*, 2011, **23**, 4636-4643.

83. L. J. Koster, M. Kemerink, M. M. Wienk, K. Maturova and R. A. Janssen, *Adv. Mater.*, 2011, **23**, 1670-1674.

84. L. J. A. Koster, V. D. Mihailetchi, H. Xie and P. W. M. Blom, *Appl. Phys. Lett.*, 2005, **87**, 203502.

85. S. R. Cowan, A. Roy and A. J. Heeger, *Phys. Rev. B*, 2010, **82**.

86. C. M. Proctor, M. Kuik and T.-Q. Nguyen, *Prog. Polym. Sci.*, 2013, **38**, 1941-1960.

87. W. Chen, T. Xu, F. He, W. Wang, C. Wang, J. Strzalka, Y. Liu, J. Wen, D. J. Miller, J. Chen, K. Hong, L. Yu and S. B. Darling, *Nano Lett*, 2011, **11**, 3707-3713.

Graphical Abstract:

Carbazole Green and Blue-BODIPY Dyads and Triads as Donors for Bulk Heterojunction Organic Solar Cells

Jian Yang, Charles H. Devillers, Paul Fleurat-Lessard, Hao Jiang, Shifa Wang, Claude P. Gros, Gaurav Gupta, Ganesh D. Sharma, and Haijun Xu

*Two BODIPY derivatives with one (**B2**) and two (**B3**) carbazole moieties were designed, synthesized and applied as electron-donor materials in organic photovoltaic cells (OPV), showing overall PCE of 6.41% and 7.47%, respectively.*